Science Advances
AAAS

advances.sciencemag.org/cgi/content/full/6/23/eaba9206/DC1

Supplementary Materials for

Nitrogen in black phosphorus structure

Cheng Ji, Adebayo A. Adeleke, Liuxiang Yang, Biao Wan, Huiyang Gou*, Yansun Yao*, Bing Li, Yue Meng, Jesse S. Smith, Vitali B. Prakapenka, Wenjun Liu, Guoyin Shen, Wendy L. Mao, Ho-kwang Mao*

*Corresponding author. Email: huiyang.gou@hpstar.ac.cn (H.G.); yansun.yao@usask.ca (Y.Y.); maohk@hpstar.ac.cn (H.-k.M.)

Published 3 June 2020, *Sci. Adv.* **6**, eaba9206 (2020)
DOI: 10.1126/sciadv.aba9206

This PDF file includes:

Supplementary Text

Calculation of Raman spectrum

The intensity for the vth Raman mode with angular frequency ω_v is calculated using Placzek approximation (*36*) implemented in Quantum ESPRESSO package (*33*),

$$I^v \propto \left|\mathbf{e}_i \cdot \vec{\mathbf{R}}^v \cdot \mathbf{e}_s\right|^2 \frac{1}{\omega_v}(n_v + 1), \quad (1)$$

where $\mathbf{e}_i$($\mathbf{e}_s$) is the polarization of the incident (scattered) radiation and n_v is the Bose-Einstein occupation factor. The Raman tensor is therefore,

$$R^v_{lm} = \sum_{k\gamma} \frac{\partial^3 \varepsilon^{\mathrm{el}}}{\partial E_l \partial E_m \partial u_{k\gamma}} \frac{w^v_{k\gamma}}{\sqrt{M_\gamma}}. \quad (2)$$

Here $\varepsilon^{\mathrm{el}}$ is the electronic energy of the system, E_l (E_m) is the lth (mth) Cartesian component of a uniform electric field. $u_{k\gamma}$ is the kth component of the displacement of the γth atom with the atomic mass M_γ. $w^v_{k\gamma}$ is the orthonormal vibrational eigenmode v which is obtained using density functional perturbation theory.

Synthesis of Sample 2 and the corresponding theoretical characterization of the Raman modes of CG-nitrogen

Sample 2 was heated at 120 GPa with a flake of graphite as laser absorber up to 3900 K using transient laser heating at 13 IDD of GSECARS. The transient heating can only be done for one time since the graphite immediately turned transparent. A relatively bulky single crystal of CG-nitrogen was synthesized. The XRD data supports the formation of pure CG-nitrogen without any trace of the BP-structured nitrogen in the sample, as shown in fig. S5A. The Raman spectrum of Sample 2 after laser heating shows a strong major peak belonging to the *A* mode with the frequency consistent to the previous studies. Because of the strong Raman signal, two additional weak features were also observed in the Raman spectrum, as shown in fig. S5B. One of the two peaks can be assigned with confidence to the low-frequency *T* mode while the other is possibly the high-frequency *T* mode (named *T'*). These modes were not observed in any previous experiment probably due to their low intensity. The presence of the two *T* modes is consistent with the group theory analysis and zone-center phonon calculation. According to the group theory, the CG-nitrogen (space group $I2_13$) should have four Raman active modes, $A + E + 2T$. The density functional perturbation calculation shows that the spectrum is dominated by the *A* mode because the intensities of the $E + 2T$ modes are less than 10% of the former and therefore hardly observable.

Estimation of the pressure conditions for synthesizing BP-structured nitrogen

The P-T conditions for synthesizing BP-structured nitrogen appear narrow. We explored the synthesis by laser heating experiments at 120 GPa, 146 GPa, 149 GPa, 160 GPa, and 190 GPa, as shown in fig. S6. At 120 GPa, we synthesized CG-nitrogen by using nitrogen with graphite laser coupler (Sample 2). At 146 GPa, BP-structured nitrogen (mixed with CG-nitrogen) was synthesized by direct laser heating nitrogen (Sample 1). At 149 GPa, BP-structured nitrogen was able to be synthesized by heating a laser coupler inside nitrogen. At 160 GPa and 190 GPa,

nitrogen directly absorbs laser irradiation and transforms to a transparent amorphous phase, as also being reported by Laniel *et al (13)*.

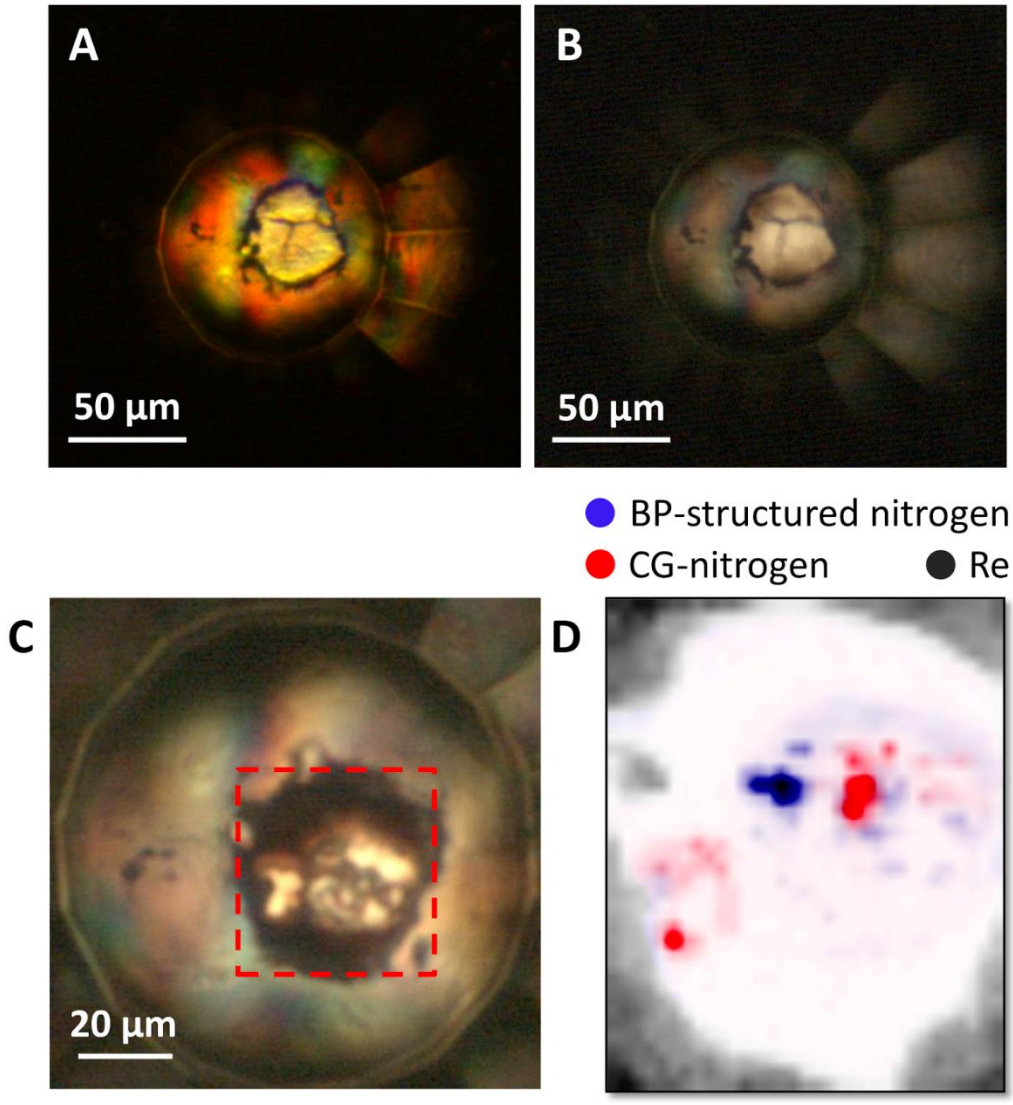

Fig. S1. Micro-images and XRD contrast imaging of Sample 1. (**A**) Micro-image at 127 GPa. (**B**) Micro-image at 150 GPa. Both A and B were collected before laser heating and with illumination with both reflected and transmitted light. (**C**) Micro-image of Sample 1 after laser heating. Red dash line box includes the sample area corresponding to the area being mapped in D. (**D**) Two-dimensional XRD contrast imaging using monochromatic focused X-ray probe with 500 nm FWHM. Blue, red, and black color represent BP-structured nitrogen, CG-nitrogen, and Re. Darker color means higher integrated XRD peak intensity, suggesting the higher content of the corresponding phase. One representative integrated XRD peak from each phase was tracked to calculate the presence of the corresponding phase. Data processing was performed by using the XDI software (*26*). Two-dimensional XRD data was collected by moving the sample in a two-dimensional grid [40 µm (vertical) by 32 µm (horizontal)] with 1 µm step size (the total data collection took approximately 10 hr). Data were collected with DAC being static without rotation. Since data at many sample positions are spotty, the intensity of the map is not reliable due to

potentially different crystal orientations at different sample positions (some crystals of a certain phase may be absent in the map since the crystal orientations do not satisfy the Bragg conditions).

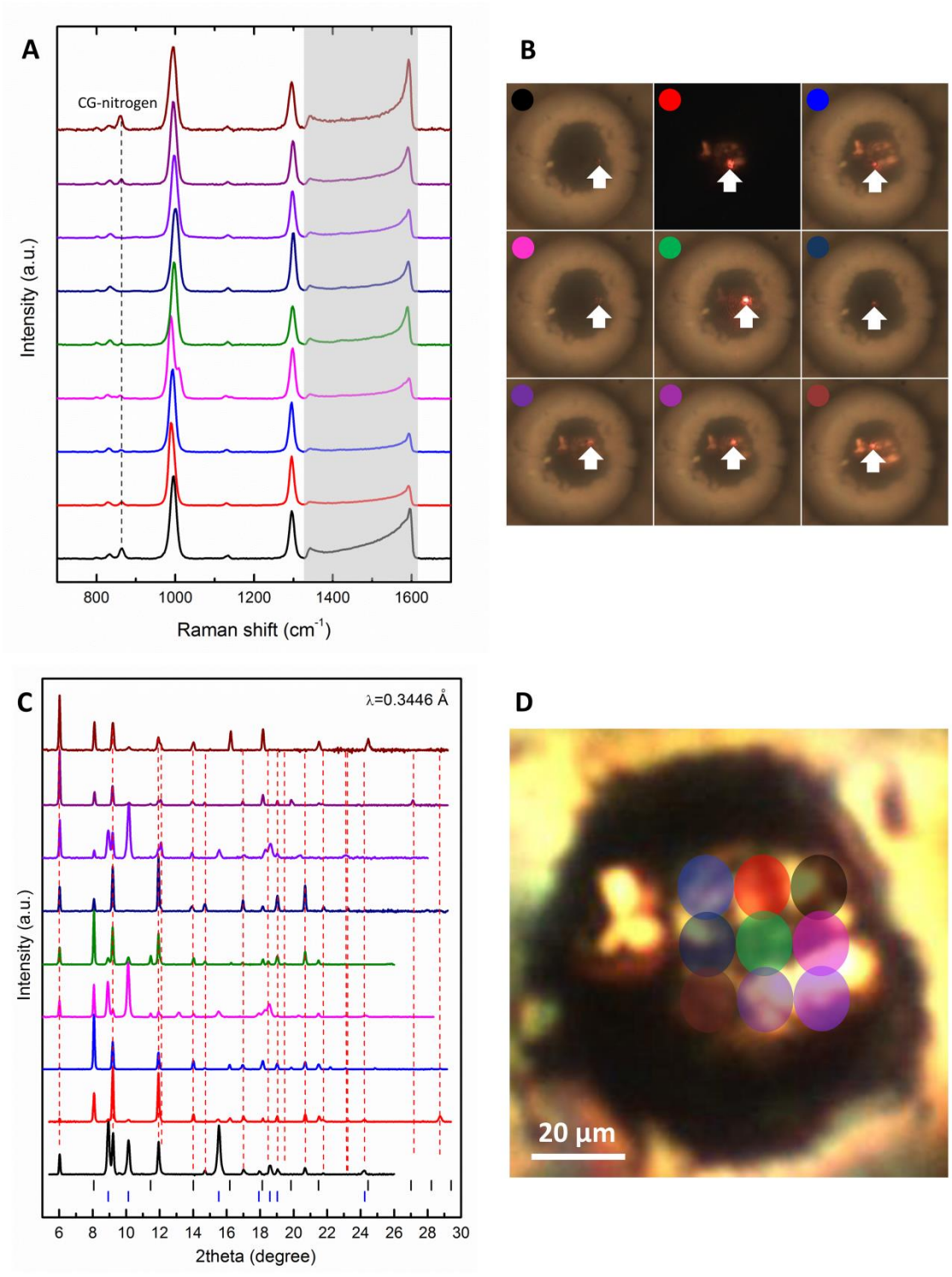

Fig. S2. Raman spectra and XRD patterns with corresponding micro-images of Sample 1 at a series of sampling positions. (**A**) Raman spectra collected at different sample positions. Dash line mark the *A* mode peak from the CG phase. Gray shade masks the Raman signal from the stressed diamond anvil. (**B**) Montage of nine micro-images showing the sample positions where the Raman spectra were measured. Spectrum in a particular color in A is measured at

the sample location in B with a marker in the corresponding color located at the left upper corner. White arrows mark the laser spot positions on the sample. (**C**) XRD patterns collected at nine different sample locations. Red dash lines mark peaks from BP-structured nitrogen. Black and blue ticks at the bottom mark peak positions from the CG-nitrogen and Re, respectively. Diffraction data were collected by widely rotating the DAC from -21 ° to +21 ° about the **Ω**-axis. Diffraction peaks from the new phases at different sample positions are overall consistent (the sample contains deformed single crystal grains with different crystal orientations, thus slightly different reflections may present at different sample positions). Patterns plotted in black, magenta, and violet show strong Re peaks due to the closeness of the sample positions to the edge of the sample chamber. (**D**) Sample positions corresponding to the XRD patterns marked by colored spots on the micro-image. XRD pattern in a particular color in C is measured at the sample location in D with the same color. Size of the spots represents the real focused XRD probe size (FWHM).

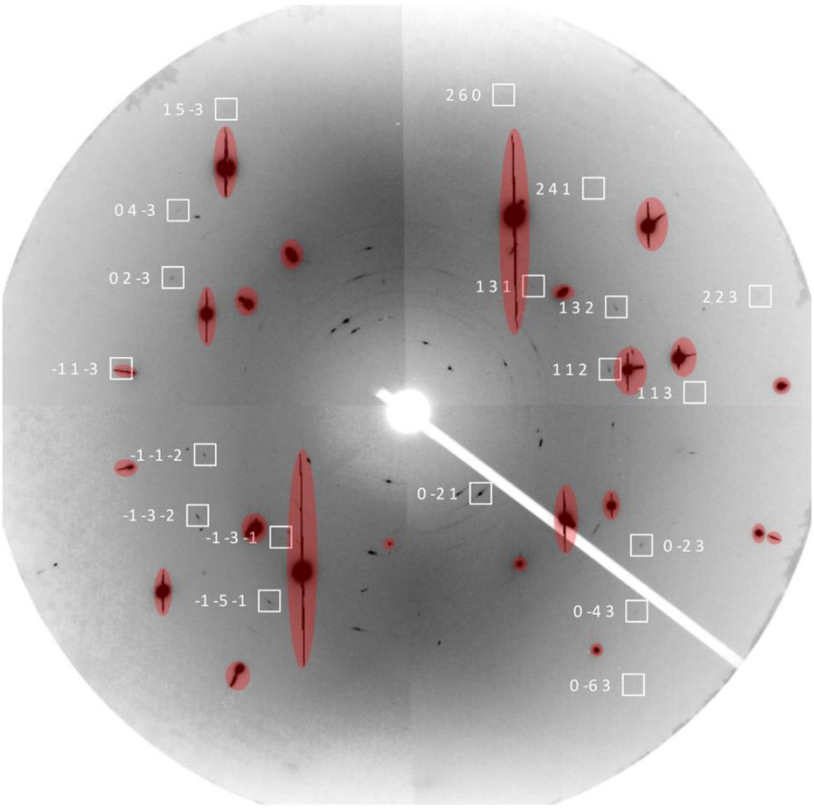

Fig. S3. Diffraction spots from the grain #1 of BP-structured nitrogen on the raw image. White boxes mark the diffraction spots. Numbers are miller indices of the corresponding XRD spots. Image is merged from step scan patterns of selected Ω angles to demonstrate BP-structured nitrogen XRD spots. Intensity of the XRD from the grain #1 is in general weaker than that of the grain #2. Some weak spots are not obvious since this pattern is obtained by merging multiple patterns, many of which do not contain the specific XRD spots. Red shades mask reflections related to diamond anvils.

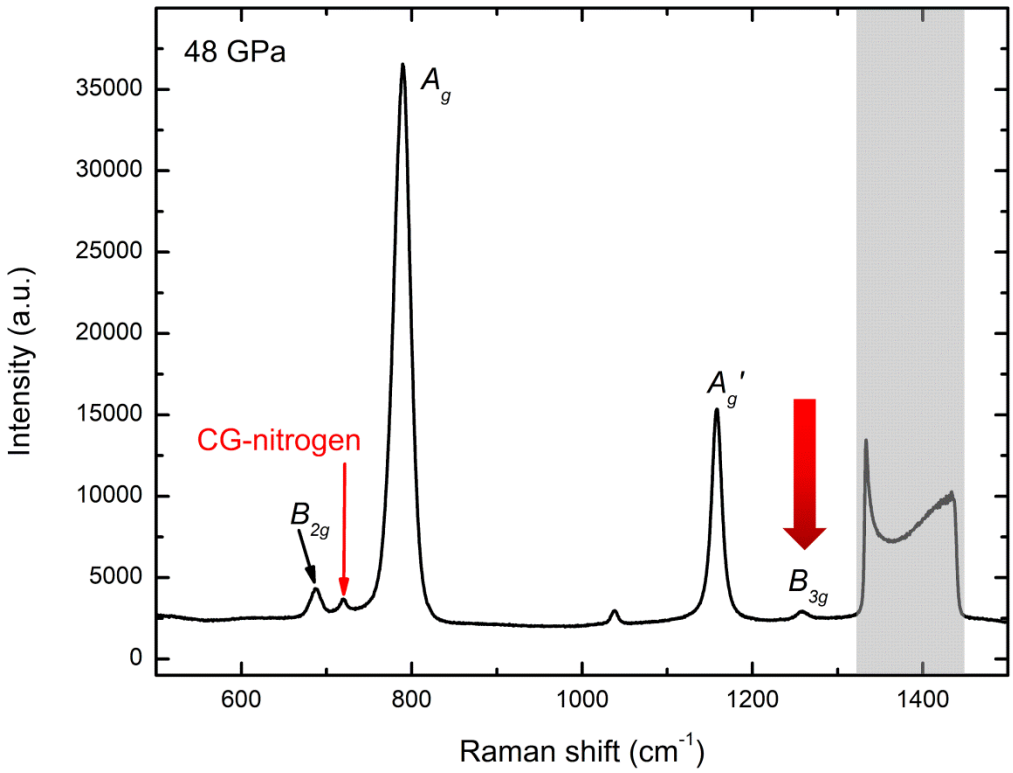

Fig. S4. Raman spectrum of the Sample 1 measured at 48 GPa upon decompression. The B_{3g} mode, overlapping with diamond Raman edge at megabar pressures, shifts out of the spectral region of diamond Raman edge at 48 GPa. Big red arrow points to the B_{3g} mode.

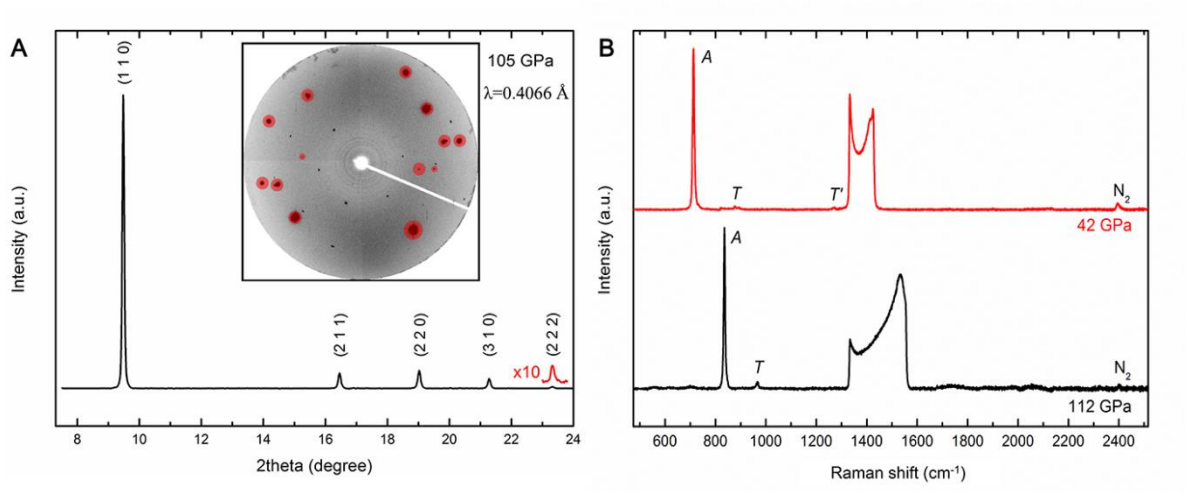

Fig. S5. Raman spectra and XRD pattern of Sample 2. (**A**) XRD pattern of the Sample 2. Five families of reflections can be well indexed with CG-nitrogen. Numbers in parenthesis are the Miller indices of the corresponding peaks. Inset shows the raw XRD image. Data was collected while widely rotating the DAC from -18° to +18° about the **Ω**-axis. Diffraction signal from CG-nitrogen is spotty. Red spots mask the diffraction from diamond anvils. (**B**) Raman spectra of Sample 2 after the synthesis and at the lowest pressure when the CG-nitrogen was still preserved. *A*, *T*, and *T'* mark the Raman modes of CG-nitrogen. N_2 mark the Raman mode from molecular nitrogen (un-reacted sample upon laser heating). The *T'* mode was buried by the Raman signal of the stressed diamond anvil at high pressure and shifted out of the diamond Raman signal upon decompression.

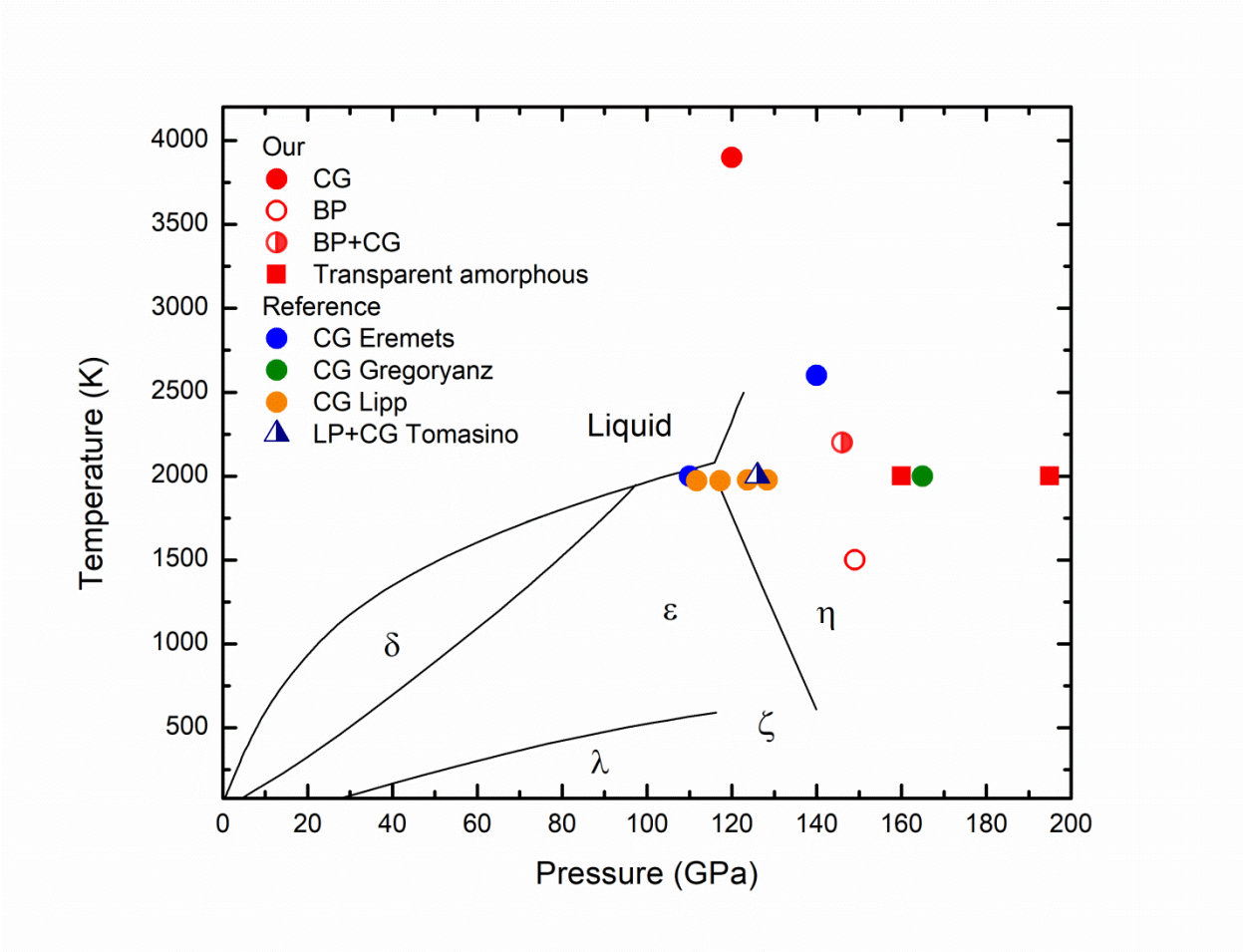

Fig. S6. Phase diagram of nitrogen and synthesis conditions of polymeric nitrogen phases. Phase diagram is adapted from literatures (*37, 38*). Red solid circle, open circle, half solid half open circle, and solid squares represent synthesis conditions of CG-nitrogen, BP-structured nitrogen, mixture of CG-nitrogen with BP-structured nitrogen, and transparent amorphous nitrogen, respectively, from our own data. Blue circles, green circle, orange circles, and navy upper triangle (half open half solid) represent synthesis conditions of CG-nitrogen from (*10*, *39*, *40*) and mixture of LP-nitrogen with CG-nitrogen from (*11*). CG, BP, and LP in figure legend represent CG-nitrogen, BP-structured nitrogen, and LP-nitrogen, respectively.

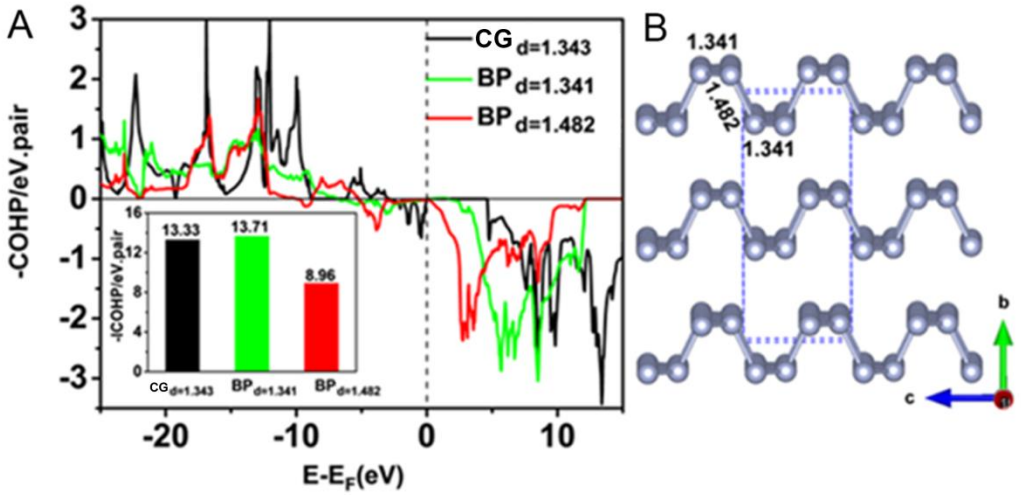

Fig. S7. Comparison of –COHP of N-N pairs between BP-structured nitrogen and CG-nitrogen at 100 GPa. (**A**) Calculated -COHP curves of N-N pairs in BP-structured nitrogen and CG-nitrogen. Insert map is the calculated -ICOHP of N-N pairs. For comparison, the -COHP value for a triple bond in N_2 is 23.07. (**B**) Crystal structure of BP-structured nitrogen at 100 GPa with bond lengths noted.

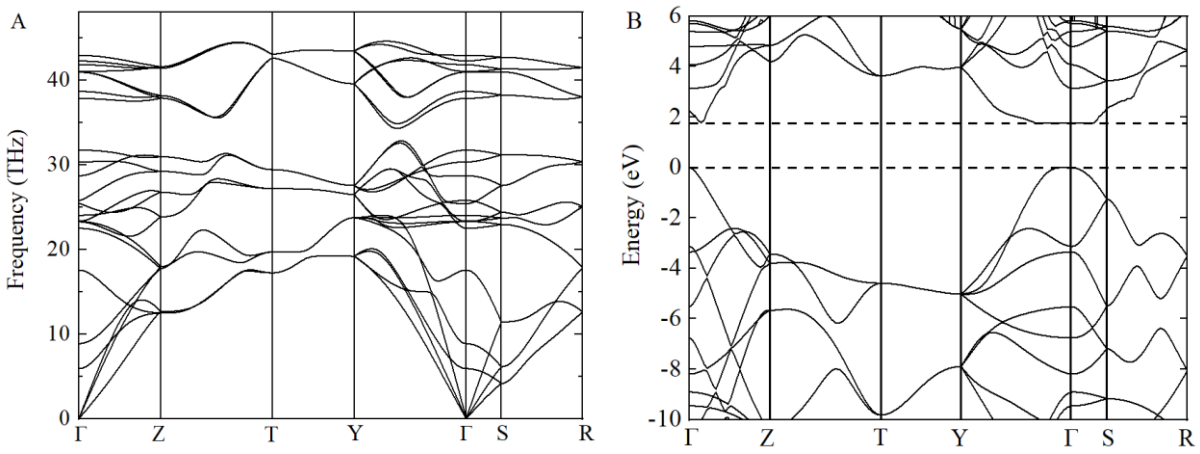

Fig. S8. Calculated (A) phonon dispersion relations and (B) band structure for BP-structured nitrogen at 150 GPa.

Table S1. Comparison of the predicted angles and the observed angles (in reciprocal space) between reflection spot 0 -2 1 and other reflection spots of the grain #1 as well as between reflection spot 0 2 0 and other reflection spots of the grain #2. Angles between two reflections according to the specific diffraction geometry were calculated based on the unit-cell parameters, assigned Miller indices hkl, and orientation matrix of the grain. Average FWHM of the rocking curve (SXRD data) for these reflections is approximately 2 °.

Grain #1			**Grain #2**		
0 -2 1 ∧ h k l	Calculated angle (°)	Observed angle (°)	0 2 0 ∧ h k l	Calculated angle (°)	Observed angle (°)
0 -2 1 ∧ 1 3 1	92.8	93.1	0 2 0 ∧ 0 -2 1	131.0	130.5
0 -2 1 ∧ -1 -3 -1	87.2	87.0	0 2 0 ∧ 0 2 1	49.0	48.4
0 -2 1 ∧ 1 1 2	59.9	60.2	0 2 0 ∧ 0 0 2	90.0	89.5
0 -2 1 ∧ -1 -1 -2	120.1	119.6	0 2 0 ∧ 0 4 1	29.9	29.5
0 -2 1 ∧ 1 3 2	76.2	76.1	0 2 0 ∧ 0 -4 1	150.1	149.6
0 -2 1 ∧ -1 -3 -2	103.8	103.6	0 2 0 ∧ 1 -3 -2	118.5	118.9
0 -2 1 ∧ -1 -5 -1	75.8	75.5	0 2 0 ∧ 1 1 -3	82.4	82.8
0 -2 1 ∧ 0 -2 3	24.9	25.4	0 2 0 ∧ 1 -1 -3	97.6	97.9
0 -2 1 ∧ 0 2 -3	155.1	154.6	0 2 0 ∧ 0 8 1	16.0	15.7
0 -2 1 ∧ 2 4 1	96.7	96.9	0 2 0 ∧ 0 -2 0	180.0	179.4
0 -2 1 ∧ 1 1 3	53.3	53.4	0 2 0 ∧ 0 -2 1	131.0	131.4
0 -2 1 ∧ -1 1 -3	140.3	139.9	0 0 2 ∧ 0 -4 0	180.0	176.4
0 -2 1 ∧ 0 4 -3	169.1	169.1	0 0 2 ∧ 0 4 0	0.0	0.3
0 -2 1 ∧ 0 -4 3	10.9	11.1			
0 -2 1 ∧ 2 6 0	117.4	117.1			
0 -2 1 ∧ 1 5 -3	159.6	159.6			
0 -2 1 ∧ 0 -6 3	0.0	0.2			
0 -2 1 ∧ 2 2 3	65.7	65.6			

Table S2. Calculated Raman tensor R_{lm}^{v} for CG-nitrogen (1) and BP-structured nitrogen (2) at 138 GPa. The *T* and *T'* modes are triple degenerate and the *E* mode is double degenerate for CG-nitrogen.

(1) R_{lm}^{v} of CG-nitrogen

A mode (*v* = 4) Frequency = 869.5 cm^{-1}

4.5874064	0.0000000	0.0000000
0.0000000	4.5874064	0.0000000
0.0000000	0.0000000	4.5874064

T mode (*v* = 5, 6, 7) Frequency = 986.8 cm^{-1}

0.0000000	-0.0384558	0.9515488
-0.0384558	0.0000000	-0.2396883
0.9515488	-0.2396883	0.0000000

0.0000000	0.0465419	-0.2378335
0.0465419	0.0000000	-0.9516528
-0.2378335	-0.9516528	0.0000000

0.0000000	0.9801684	0.0486264
0.9801684	0.0000000	0.0357842
0.0486264	0.0357842	0.0000000

E mode (*v* = 8, 9) Frequency = 1372.7 cm^{-1}

-0.1181099	0.0000000	0.0000000
0.0000000	-0.2746768	0.0000000
0.0000000	0.0000000	0.3927867

0.3853607	0.0000000	0.0000000
0.0000000	-0.2949658	0.0000000
0.0000000	0.0000000	-0.0903933

T' mode (*v* = 10, 11, 12) Frequency = 1501.2 cm^{-1}

0.0000000	0.7931578	0.1423568
0.7931578	0.0000000	-0.1804449
0.1423568	-0.1804449	0.0000000

0.0000000	0.0180929	-0.6849812
0.0180929	0.0000000	-0.4608662
-0.6849812	-0.4608662	0.0000000

0.0000000	-0.2291255	0.4387023
-0.2291255	0.0000000	-0.6610340
0.4387023	-0.6610340	0.0000000

(2) R_{lm}^{v} of BP-structured nitrogen

B_{1g} mode (v = 5) Frequency = 799.8 cm^{-1}

0.0000000	-6.8210556	0.0000000
-6.8210556	0.0000000	0.0000000
0.0000000	0.0000000	0.0000000

B_{2g} mode (v = 6) Frequency = 818.6 cm^{-1}

0.0000000	0.0000000	0.0000000
0.0000000	0.0000000	16.9831027
0.0000000	16.9831027	0.0000000

A_g mode (v = 7) Frequency = 977.8 cm^{-1}

16.7898916	0.0000000	0.0000000
0.0000000	21.8598733	0.0000000
0.0000000	0.0000000	139.2992139

B_{2g}' mode (v = 8) Frequency = 1053.4 cm-1

0.0000000	0.0000000	0.0000000
0.0000000	0.0000000	10.8787838
0.0000000	10.8787838	0.0000000

A_g' mode (v = 9) Frequency = 1290.8 cm-1

7.6177221	0.0000000	0.0000000
0.0000000	4.1704502	0.0000000
0.0000000	0.0000000	103.4467104

B_{3g} mode (v = 12) Frequency = 1430.9 cm-1

0.0000000	0.0000000	33.5848116
0.0000000	0.0000000	0.0000000
33.5848116	0.0000000	0.0000000

REFERENCES AND NOTES

1. A. F. Goncharov, E. Gregoryanz, H. K. Mao, Z. Liu, R. J. Hemley, Optical evidence for a nonmolecular phase of nitrogen above 150 GPa. *Phys. Rev. Lett.* **85**, 1262–1265 (2000).

2. M. I. Eremets, R. J. Hemley, H.-k. Mao, E. Gregoryanz, Semiconducting non-molecular nitrogen up to 240 GPa and its low-pressure stability. *Nature* **411**, 170–174 (2001).

3. E. Gregoryanz, A. F. Goncharov, R. J. Hemley, H.-k. Mao, High-pressure amorphous nitrogen. *Phys. Rev. B* **64**, 052103 (2001).

4. X. Ling, H. Wang, S. Huang, F. Xia, M. S. Dresselhaus, The renaissance of black phosphorus. *Proc. Natl. Acad. Sci. U.S.A.* **112**, 4523–4530 (2015).

5. A. Carvalho, M. Wang, X. Zhu, A. S. Rodin, H. Su, A. H. Castro Neto, Phosphorene: From theory to applications. *Nat. Rev. Mater.* **1**, 16061 (2016).

6. F. Xia, H. Wang, J. C. M. Hwang, A. H. C. Neto, L. Yang, Black phosphorus and its isoelectronic materials. *Nat. Rev. Phys.* **1**, 306–317 (2019).

7. I. K. Drozdov, A. Alexandradinata, S. Jeon, S. Nadj-Perge, H. Ji, R. J. Cava, B. A. Bernevig, A. Yazdani, One-dimensional topological edge states of bismuth bilayers. *Nat. Phys.* **10**, 664–669 (2014).

8. M. Pumera, Z. Sofer, 2D monoelemental arsenene, antimonene, and bismuthene: Beyond black phosphorus. *Adv. Mater.* **29**, 1605299 (2017).

9. C. Mailhiot, L. H. Yang, A. K. McMahan, Polymeric nitrogen. *Phys. Rev. B* **46**, 14419–14435 (1992).

10. M. I. Eremets, A. G. Gavriliuk, I. A. Trojan, D. A. Dzivenko, R. Boehler, Single-bonded cubic form of nitrogen. *Nat. Mater.* **3**, 558–563 (2004).

11. D. Tomasino, M. Kim, J. Smith, C.-S. Yoo, Pressure-induced symmetry-lowering transition in dense nitrogen to layered polymeric nitrogen (LP-N) with colossal Raman intensity. *Phys. Rev. Lett.* **113**, 205502 (2014).

12. Y. Ma, A. R. Oganov, Z. Li, Y. Xie, J. Kotakoski, Novel high pressure structures of polymeric nitrogen. *Phys. Rev. Lett.* **102**, 065501 (2009).

13. D. Laniel, G. Geneste, G. Weck, M. Mezouar, P. Loubeyre, Hexagonal layered polymeric nitrogen phase synthesized near 250 GPa. *Phys. Rev. Lett.* **122**, 066001 (2019).

14. L. Zhang, H. Yuan, Y. Meng, H.-K. Mao, Development of high-pressure multigrain X-ray diffraction for exploring the Earth's interior. *Engineering*, **5**, 441–447 (2019).

15. T. Kikegawa, H. Iwasaki, An x-ray diffraction study of lattice compression and phase transition of crystalline phosphorus. *Acta Crystallogr.* **B39**, 158–164 (1983).

16. E. M. Benchafia, Z. Yao, G. Yuan, T. Chou, H. Piao, X. Wang, Z. Iqbal, Cubic gauche polymeric nitrogen under ambient conditions. *Nat. Commun.* **8**, 930 (2017).

17. F. Zahariev, A. Hu, J. Hooper, F. Zhang, T. Woo, Layered single-bonded nonmolecular phase of nitrogen from first-principles simulation. *Phys. Rev. B* **72**, 214108 (2005).

18. A. A. Adeleke, M. J. Greschner, A. Majumdar, B. Wan, H. Liu, Z. Li, H. Gou, Y. Yao, Single-bonded allotrope of nitrogen predicted at high pressure. *Phys. Rev. B* **96**, 224104 (2017).

19. W. D. Mattson, D. Sanchez-Portal, S. Chiesa, R. M. Martin, Prediction of new phases of nitrogen at high pressure from first-principles simulations. *Phys. Rev. Lett.* **93**, 125501 (2004).

20. A. R. Oganov, C. W. Glass, Crystal structure prediction using ab initio evolutionary techniques: Principles and applications. *J. Chem. Phys.* **124**, 244704 (2006).

21. C. J. Pickard, R. J. Needs, High-pressure phases of nitrogen. *Phys. Rev. Lett.* **102**, 125702 (2009).

22. O. L. Anderson, D. G. Isaak, S. Yamamoto, Anharmonicity and the equation of state for gold. *J. Appl. Phys.* **65**, 1534 (1989).

23. Y. Akahama, H. Kawamura, Pressure calibration of diamond anvil Raman gauge to 410 GPa. *J. Phys. Conf. Ser.* **215**, 012195 (2010).

24. N. Holtgrewe, E. Greenberg, C. Prescher, V. B. Prakapenka, A. F. Goncharov, Advanced integrated optical spectroscopy system for diamond anvil cell studies at GSECARS. *High Pressure Res.* **39**, 457–470 (2019).

25. B. H. Toby, EXPGUI, a graphical user interface for GSAS. *J. Appl. Crystallogr.* **34**, 210–213 (2001).

26. R. Hrubiak, J. S. Smith, G. Shen, Multimode scanning X-ray diffraction microscopy for diamond anvil cell experiments. *Rev. Sci. Instrum.* **90**, 025109 (2019).

27. C. Prescher, V. B. Prakapenka, *DIOPTAS*: A program for reduction of two-dimensional X-ray diffraction data and data exploration. *High Pressure Res.* **35**, 223–230 (2015).

28. M. Wojdyr, Fityk: A general-purpose peak fitting program. *J. Appl. Crystallogr.* **43**, 1126–1128 (2010).

29. J. Gonzalez-Platas, M. Alvaro, F. Nestola, R. Angel, EosFit7-GUI: A new graphical user interface for equation of state calculations, analyses and teaching. *J. Appl. Crystallogr.* **49**, 1377–1382 (2016).

30. G. Kresse, J. Hafner, *Ab initio* molecular dynamics for liquid metals. *Phys. Rev. B* **47**, 558–561 (1993).

31. G. Kresse, D. Joubert, From ultrasoft pseudopotentials to the projector augmented-wave method. *Phys. Rev. B* **59**, 1758–1775 (1999).

32. J. P. Perdew, K. Burke, M. Ernzerhof, Generalized gradient approximation made simple. *Phys. Rev. Lett.* **77**, 3865–3868 (1996).

33. P. Giannozzi, O. Andreussi, T. Brumme, O. Bunau, M. Buongiorno Nardelli, M. Calandra, R. Car, C. Cavazzoni, D. Ceresoli, M. Cococcioni, N. Colonna, I. Carnimeo, A. Dal Corso, S. de Gironcoli, P. Delugas, R. A. DiStasio, A. Ferretti, A. Floris, G. Fratesi, G. Fugallo, R. Gebauer, U. Gerstmann, F. Giustino, T. Gorni, J. Jia, M. Kawamura, H. Y. Ko, A. Kokalj, E. Küçükbenli, M. Lazzeri, M. Marsili, N. Marzari, F. Mauri, N. L. Nguyen, H. V. Nguyen, A. Otero-de-la-Roza, L. Paulatto, S. Poncé, D. Rocca, R. Sabatini, B. Santra, M. Schlipf, A. P. Seitsonen, A. Smogunov, I. Timrov, T. Thonhauser, P. Umari, N. Vast, X. Wu, S. Baroni, Advanced capabilities for materials modelling with Quantum ESPRESSO. *J. Phys. Condens. Matter* **29**, 465901 (2017).

34. S. Maintz, V. L. Deringer, A. L. Tchougreeff, R. Dronskowski, LOBSTER: A tool to extract chemical bonding from plane-wave based DFT. *J. Comput. Chem.* **37**, 1030–1035 (2016).

35. J. Heyd, G. E. Scuseria, M. Ernzerhof, Hybrid functionals based on a screened Coulomb potential. *J. Chem. Phys.* **118**, 8207 (2003).

36. M. Lazzeri, F. Mauri, First-principles calculation of vibrational Raman spectra in large systems: Signature of small rings in crystalline SiO_2. *Phys. Rev. Lett.* **90**, 036401 (2003).

37. R. Turnbull, M. Hanfland, J. Binns, M. Martinez-Canales, M. Frost, M. Marqués, R. T. Howie, E. Gregoryanz, Unusually complex phase of dense nitrogen at extreme conditions. *Nat. Commun.* 9, 4717 (2018).

38. G. Weck, F. Datchi, G. Garbarino, S. Ninet, J.-A. Queyroux, T. Plisson, M. Mezouar, P. Loubeyre, Melting curve and liquid structure of nitrogen probed by X-ray diffraction to 120 GPa. *Phys. Rev. Lett.* **119**, 235701 (2017).

39**.** E. Gregoryanz, A. F. Goncharov, C. Sanloup, M. Somayazulu, H. K. Mao, R. J. Hemley, High P-T transformations of nitrogen to 170 GPa. *J. Chem. Phys.* **126**, 184505 (2007).

40. M. J. Lipp, J. Park Klepeis, B. J. Baer, H. Cynn, W. J. Evans, V. Iota, C.-S. Yoo, Transformation of molecular nitrogen to nonmolecular phases at megabar pressures by direct laser heating. *Phys. Rev. B* **76**, 014113 (2007).